Progress In Electromagnetics Research C, Vol. 71, 79–89, 2017

Enhanced Low Profile, Dual-Band Antenna via Novel Electromagnetic Band Gap Structure

Mohammad El Ghabzouri[1, *], Abdenacer Es Salhi[1], Pedro Anacleto[2], and Paulo M. Mendes[2]

Abstract—This paper presents a dual-band, low profile antenna with reduced specific absorption rate (SAR) for mobile handset applications. Here, dual-band operation is obtained by combining a printed dipole antenna (initially resonating at 4.3 GHz) with EBG mushroom-like structures loaded with circular slots (CS). The final structure operates at 3.44 GHz (additional band required for LTE Advanced LTE-A) and 4.5 GHz (for Smartphone WLAN applications) with improved bandwidth and reflection coefficient (350-MHz around 3.5 GHz with −26 dB, and 330 MHz around 4.5 GHz with −30 dB). Finally, a dosimetry study of the proposed printed dual-band dipole antenna is presented and verifies an SAR reduction from 9 W/Kg to 1.41 W/Kg compared to the same antenna without any loading structure, and from 3.98 W/Kg to 1.41 W/Kg compared to a standard EBG mushroom-like structure.

1. INTRODUCTION

The acceptance of electromagnetic band gap (EBG) structures in the microwave and antenna community, paired with the demand for sophisticated antennas that can effectively respond to the requirements of wireless device requirements and quality of service (QoS), leads researchers to investigating and analysing numerous types of EBG structures, and proposing new configurations and applications for these structures. Many have studied the Sievenpiper structure, which is known as mushroom-like structure [1–13]. Due to their particular features such as the attenuating mutual coupling and high directivity, EBG structures were found to be very useful when being combined with antennas, and soon practical applications were proposed, such as their use as a ground plane on a curl antenna to obtain circular polarisation and a low profile [2], or their effectiveness on coupling reduction between two patch antennas placed above a EBG mushroom-like structure [3]. Following works used modified versions of the original Sievenpiper structure in order to enhance particular antenna features such as the improvement of antenna patch properties [4, 5]. Afterwards, several works were dedicated to mitigation problems associated with limitations of EBG structures, such as the bandwidth drawback when combining those structures with patch antennas [6], and more recently to the theoretical study of the radiated fields [7]. Others have studied the combination of EBG with antennas for SAR reduction [8], radar cross section reduction [9] and their use as filter building block [10]. Therefore, some recent works recourse to the EBG structures, to obtain high gain and wide band [23] and also conceive a multi-band circular polarization antenna [24].

Based on our previous work [11, 12], this paper proposes a new EBG design to be combined with a dipole antenna, thus targeting dual-band, low profile, and high performance antenna, while at the same time decreasing SAR levels. The operating frequencies were selected to match operating bands of different mobile communication applications. The first band, at 3.5 GHz, is generally required for

Received 9 November 2016, Accepted 11 January 2017, Scheduled 2 February 2017
* Corresponding author: Mohammad El Ghabzouri (elghabzouri.mad@gmail.com).
[1] LESPRE Department of Physics, Faculty of science, Mohammed I University, Oujda, Morocco. [2] CMEMS, University of Minho, Guimarães, Portugal.

worldwide interoperability for microwave access (WiMAX) operation, or for one of the 4G band numbers 22, 42 and 43 allowed for LTE. Whereas the second band, around 4.5 GHz, is required for WLAN operability of handsets, or any other function inside C band.

The present paper proposes a solution to obtain dual-band antennas through the simultaneous use of an antenna and an EBG structure. The proposed EBG was designed with circular slots (CS) and loaded with a superstrate, and the combination of the EBG-CS structure with the superstrate led to actual dual-band operation. The antenna distance from the EBG-CS was also investigated as an enhancing mechanism for bandwidth and reflection coefficient. The circular slot loading on the EBG structure cells contributed to the improvement of the S_{11} (dB) and bandwidth, and the open area due to these slots also facilitated the radiation of the antennas.

2. ANTENNA DESIGN FOR DUAL BAND OPERATION

The proposed antenna design strategy consisted of three steps: first by modelling the EBG structure that conveys the band gap operation around the working frequency of the antenna. Here, the main challenge was to design the smallest structure possible with correct properties. Afterwards, a dipole antenna and a printed dipole antenna were modelled to operate at 4.3 GHz. The final step was the performance analysis of the antenna combined with the EBG, and its optimization in order to attain the dual band function, leading to an EBG-CS geometry with enhanced antenna features.

2.1. EBG Design and Analysis

The literature provides a few methods to analyse EBG structures, specifically how to identify their band gaps [13]. One methodology, based on the dispersion diagram, relies on studying the wave vector in function of frequency. This identification technique is more commonly used when being solved by the FDTD (Finite Deference Time Domain) method. The dispersion diagram can also be calculated using an eigen mode solver to draw a band gap [14]. The reflection phase is also a widely used method that allows the characterization of a unit cell, and from that on, to the identification of the band gap. This method is based on the reflection phase curve extraction, which can then be used to see if the band gap criterion is met between 0° and 180° or ±45° [15].

Despite the effectiveness of the aforementioned methods, a faster and more straightforward technique to identify the band gap of the proposed structures (EBG mushroom-like and EBG with circular slots EBG-CS) is known as 50 ohm suspended line. The key aspect of this method is to model

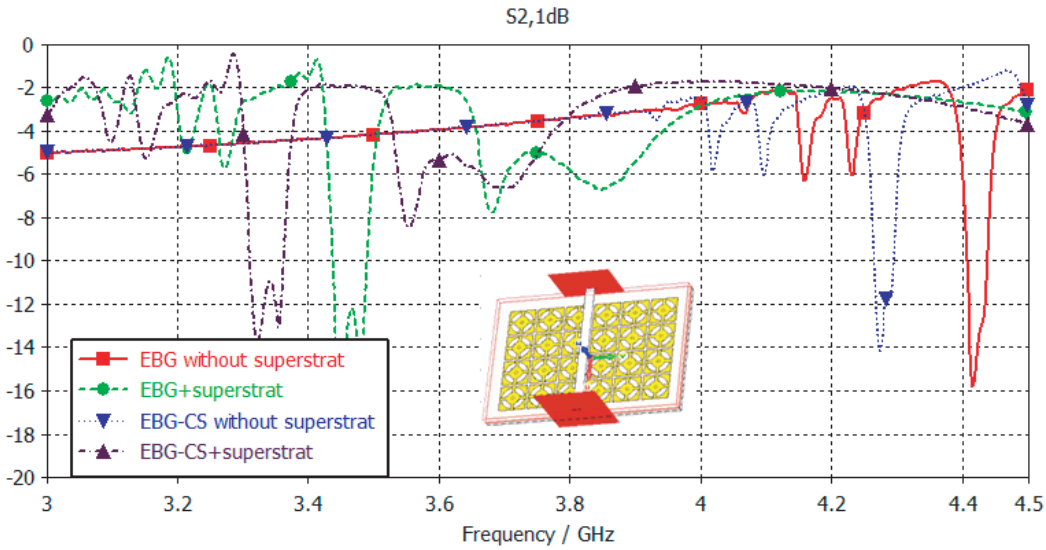

Figure 1. EBG-CS and EBG mushroom like performance comparison, with and without superstrate.

the whole structure and then insert a microstrip line on top of the test structure (EBG-CS plus the superstrate). To complete the design and in order to obtain the transmission parameter S_{21}, both ends of the microstrip line over the model are fed with waveguide ports to transmit and receive electromagnetic waves [25].

Figure 1 shows the transmission parameter S_{21} obtained from the standard EBG mushroom-like and EBG-CS structures. This configuration was obtained after having examined the standard square patch cells with multiple options of slot shapes, and a refinement process for frequency optimization, improved bandwidth and radiation efficiency.

S_{21} values of the proposed structures, with and without superstrate, are shown in Fig. 1. It can be seen that by loading the EBG or EBG-CS with a superstrate, the band gaps move to a lower frequency, which allows shrinking the expected size of the initial superstrate-free EBG. In this way, the proposed structure helps maintaining a low profile device.

The geometry that rendered the best antenna performance was the EBG-CS configuration shown in inset of Fig. 1, as well in Fig. 2, where it is combined with the proposed antenna.

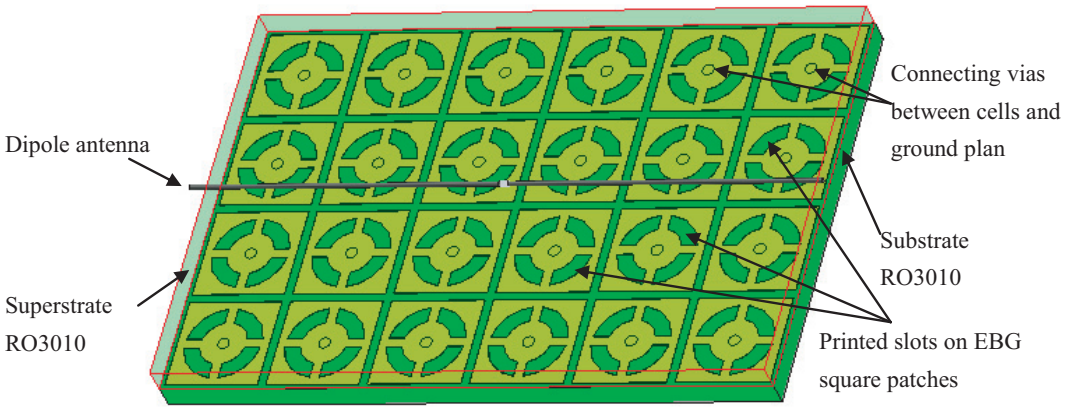

Figure 2. Setup used to transform the single band into a dual band antenna (The dimensions of the structure are given as follow: length = 33 mm, width = 21 mm, substrate and superstrate thickness = 1.27 mm).

2.2. Antenna Design

The next step was to design an antenna to interact with the EBG-CS. To be combined with the proposed EBG and EBG-CS structures, the antenna was designed considering that it would be mounted on top of the EBG superstrate. A printed half-wave dipole antenna was used [17–21], resonating around 4.3 GHz. The idea was to have the antenna operating at two new frequencies when being placed close to the EBG-CS structures. Thus, by trimming the distance between the antenna and EBG-CS, and reducing the EBG-CS size, it was possible to obtain new operating frequencies around 3.44 GHz and 4.5 GHz ($L = 0.37 * \lambda$, where λ is the wavelength of free space of the new first resonance, which contributed to an antenna miniaturisation of 26%).

The materials chosen as substrate and superstrate were Rogers RO3010 (with dielectric constant 10.2 and standard thickness of 1.27 mm). Fig. 2 shows the dipole antenna above the proposed EBG and circular slotted EBG-CS structure.

3. ANTENNA OPERATION

3.1. Operating Frequency and Bandwidth

The computed S_{11} (dB) of the dipole antenna in three situations is presented in Fig. 3: (a) above the EBG-CS structure, (b) above EBG mushroom-like structure, (c) without the EBG. The red (a) and

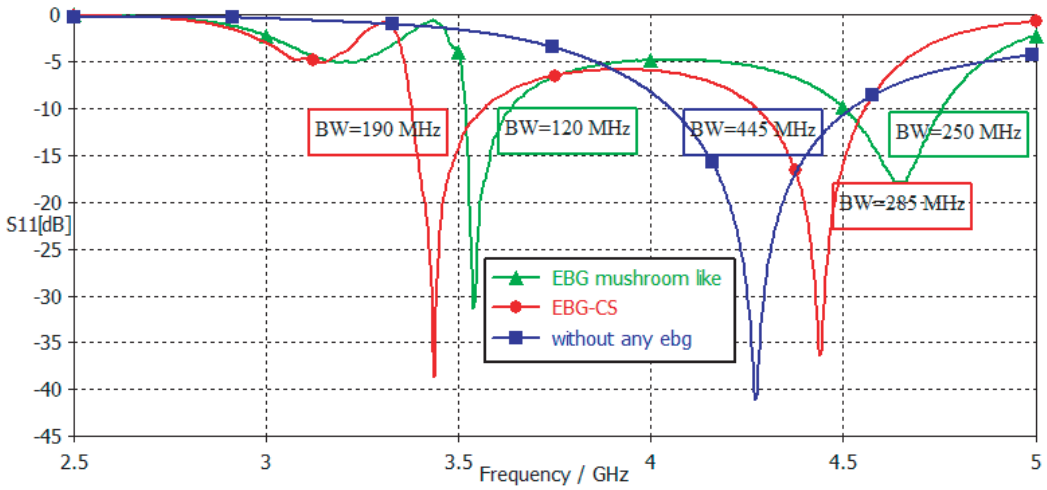

Figure 3. The reflection coefficients of a dipole antenna (a) on a EBG-CS structure (red circles), (b) on a EBG mushroom-like structure (green triangles), (c) without EBG structure (blue squares).

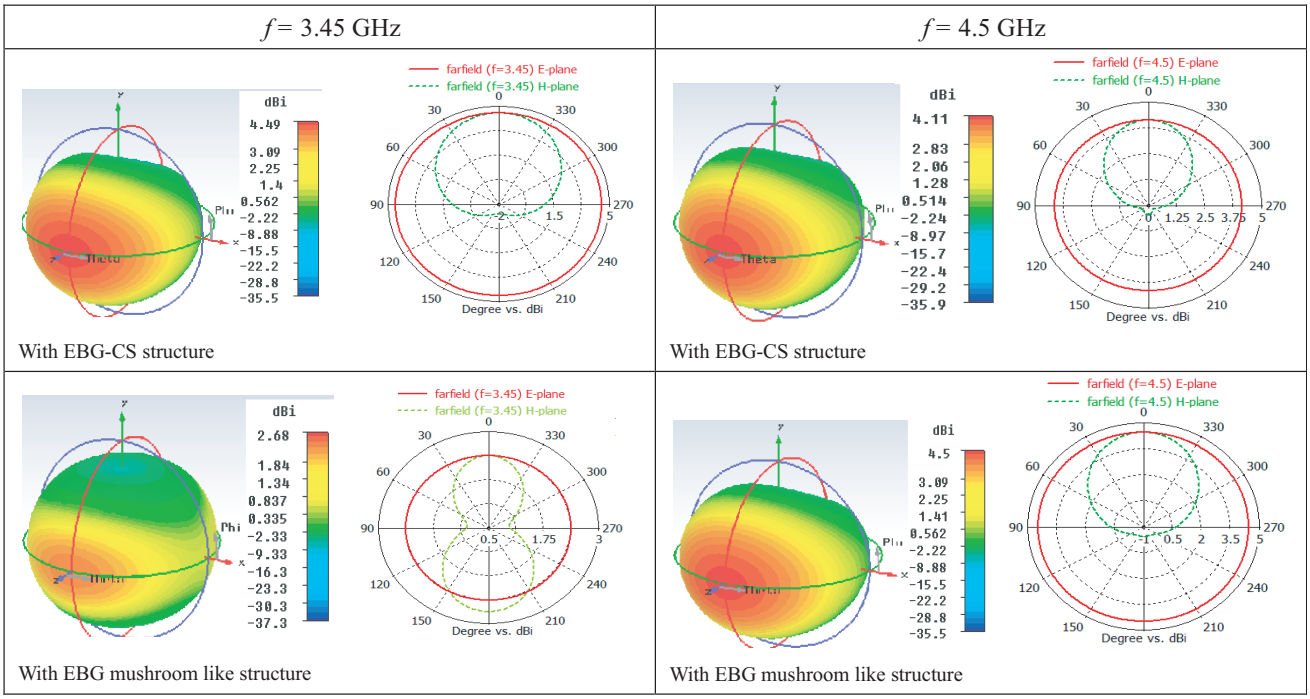

Figure 4. Directivity radiation pattern performance comparison of the EBG-CS and EBG mushroom-like structures at 3.45 GHz and 4.5 GHz.

green (b) curves represent the dual-band antenna operation, compared to the same antenna operating without the EBG structure, which is represented by the blue curve (c). When comparing the EBG-CS with the EBG mushroom-like structure, the antenna reflection coefficient and bandwidth improvements are very clear. The proposed EBG-CS structure presents a bandwidth improvement of 58.3% compared with the conventional EBG mushroom-like structure for the first resonance, and an improvement of 12% for the second band. For the EBG-CS structure, as can be seen in S_{11} (dB) minimum of -40 dB is at 3.45 GHz and that of -35 dB at 4.5 GHz.

The simulation results of the radiation pattern are also a good performance indicator of the antenna-

EBG-CS combined structure. Fig. 4 shows the 3D radiation pattern comparison for the EBG-CS and EBG mushroom-like structures at 3.45 GHz and 4.5 GHz. A directivity improvement at 3.45 GHz can also be seen, while the directivity at 4.5 GHz remains roughly the same. In addition of the directivity diagram, Fig. 4 illustrates the E-planes in red solid lines and H-planes in green dashed lines at each studied case.

3.2. SAR Calculation and Reduction

In this section, the ability of the proposed EBG-CS structure to reduce the specific absorption rate (SAR) will be studied. Since wireless devices may have an impact on our health, due to the exposure to electromagnetic waves, handheld devices are required to meet the specific SAR regulations [22].

In our experiments, the antenna output power was fixed at 1 W, and the tissue properties were selected to simulate frequencies between 3.5 GHz and 4.5 GHz. Finally, the distances (antenna-phantom head) were fixed at 10 mm. Fig. 5 shows that the SAR inside the head phantom due to EBG-CS was smaller than the SAR resulting from the EBG mushroom-like structure. The ensured low SAR can be explained by the capacity of the EBG-CS to delete more surface and parasitic waves. The loaded slots on the EBG cells also guaranteed the enhancement of the radiation pattern. These slots, besides allowing dual-band operation, also enable the control of the radiation efficiency, resonance frequency fine-tuning, as well as reaching a low S_{11} (dB) and increased bandwidths.

The results, presented in both Fig. 5 and Table 1, clearly demonstrate that our structure can contribute to SAR reduction inside human head.

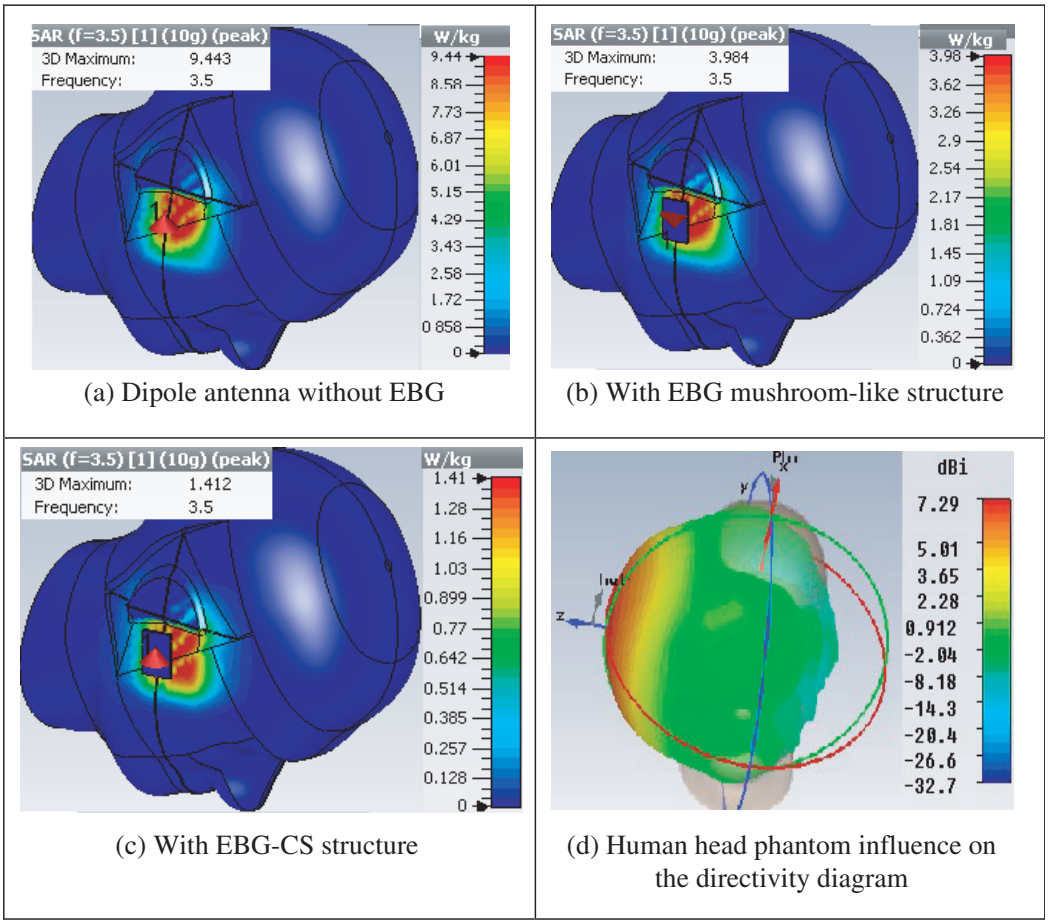

(a) Dipole antenna without EBG

(b) With EBG mushroom-like structure

(c) With EBG-CS structure

(d) Human head phantom influence on the directivity diagram

Figure 5. SAR cartography distributions of dipole antenna: (a) without EBG, (b) with EBG structure mushroom-like, (c) with the EBG-CS structure. (d) The directivity diagram.

Table 1. SAR distributions inside the human head tissues when exposed to 4G using the "IEEE C95.3 averaging method".

	SAR (Av 1g)	SAR (Av 10g)	Gain	Frequency
Without EBG	24.2 W/kg	9.44 W/kg	7.29 dBi	3.5 GHz
With EBG mushroom	10.1 W/kg	3.98 W/kg	6.95 dBi	3.5 GHz
With the proposed EBG-CS	6.63 W/kg	1.41 W/kg	7.05 dBi	3.5 GHz

4. FABRICATION AND MEASUREMENT

4.1. EBG-CS Antenna Prototype

To test the proposed EBG-CS system, a prototype that places together the developed EBG-CS and a dipole antenna was designed, simulated, and tested. Fig. 6 shows the design layout, and Fig. 7 shows EBG-CS assembled prototype.

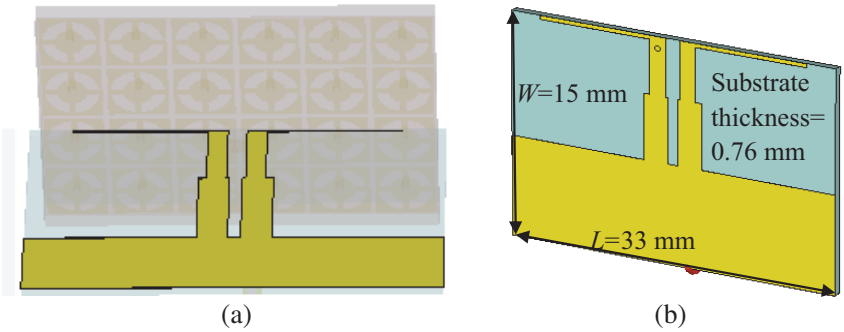

Figure 6. (a) Layout of the proposed EBG-CS antenna. (b) Antenna dimension.

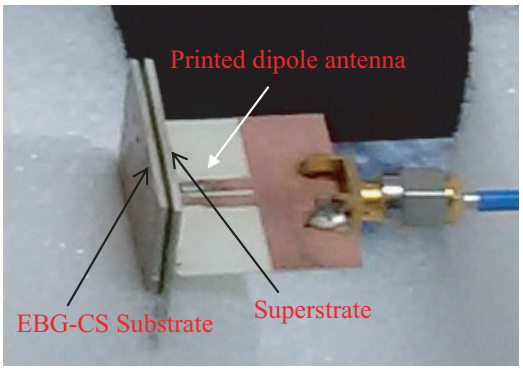

Figure 7. Fabricated prototype of the printed dipole antenna and EBG-CS zoomed from the Fig. 8.

The proposed solution uses a printed dipole antenna, fabricated on top of the proposed EBG-CS structure.

4.2. Antenna Reflection Coefficient

Figure 8 shows the setup used for antenna S_{11} (dB) measurement. Fig. 9 illustrates the simulated results of the printed dipole antenna above the EBG-CS structure (red) and the EBG mushroom-like structure (green), along with the measured results of the fabricated antenna above EBG-CS structure (blue).

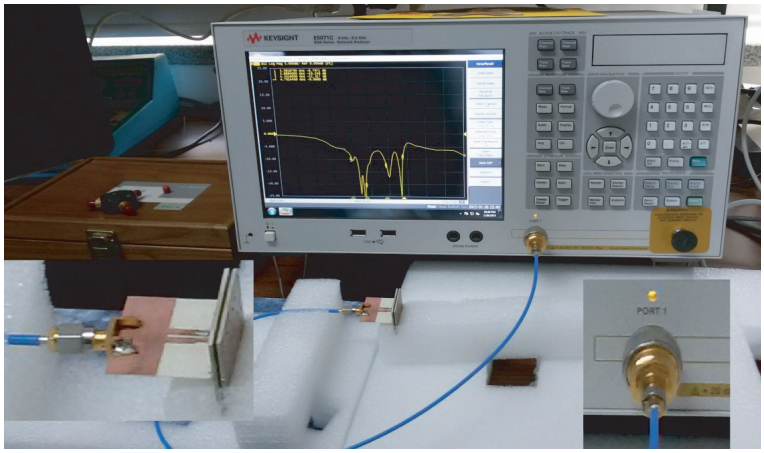

Figure 8. Setup used for the S_{11} (dB) measurement of the printed dipole antenna mounted on EBG-CS structure.

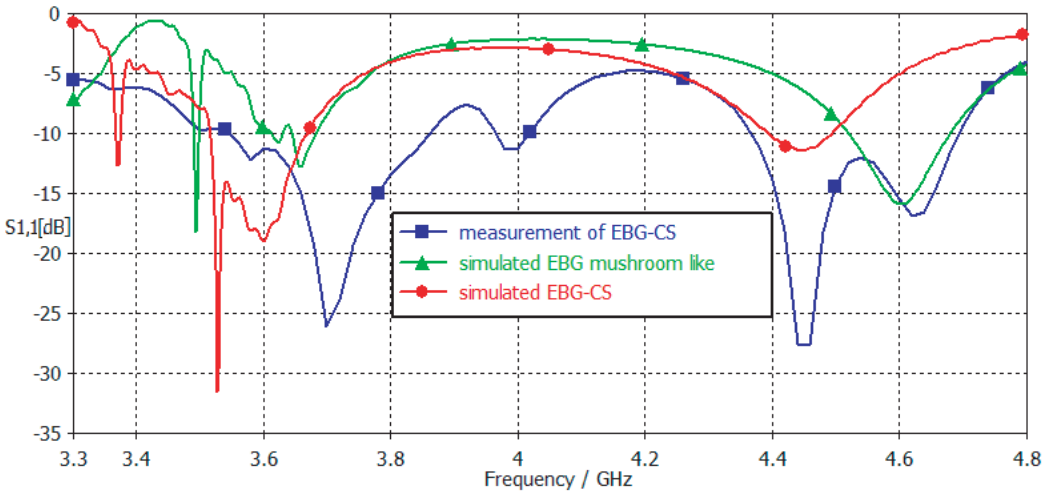

Figure 9. Simulated S_{11} of the printed dipole antenna above EBG-CS structure (red circles), and above EBG mushroom-like structure (green triangles) and the measured S_{11} of the fabricated antenna above EBG-CS structure (blue squares).

The novelty, which is emphasized in this article and has been proven and validated through experimental measurements, is the antenna dual-band behaviour. The proposed antenna was designed and fabricated to resonate around 4.3 GHz as a standalone system. However, when being combined with the EBG-CS it demonstrates dual-band operation. Fig. 9 illustrates a clear bandwidth improvement with the addition of developed EBG-CS system, as well as satisfactory agreement between simulated and measured results.

The proposed antenna, EBG-CS and superstrate combination enables not only an excellent antenna performance, but also a lightweight and low profile device. In Table 2, a comparison is shown between our system and other similar works found in the literature. It can be seen that our system has the smallest volume of them all, being only surpassed in terms of number of frequency bands by the system presented in [19], which is roughly 10 times bigger than ours.

4.3. SAR Study and Compared Results

Smartphone devices are commonly used for internet access so kept mostly in our hands. As a result, the hands are the part of the human body exposed most to electromagnetic waves. Therefore, to further

Table 2. Size reduction compared with some literature widespread EBG antennas.

	Width	Gap	Height	Volume	Resonance frequency	Ref.
EBG mushroom like	7 mm	1 mm	4.5 mm	5.29 cm^3	3.5 GHz One band	[16]
EBG circular patches	9 mm	1 mm	7.5 mm	14.5 cm^3	3.5 GHz One band	[20]
This work — EBG-CS	4.8 mm	0.4 mm	3 mm	1.65 cm^3	Dual band (3.5 & 4.5) GHz	
Square Sierpinski Fractal EBG	Total width and length = 80 * 80 mm		1.6 mm	10.24 cm^3	3 narrow bands at 2.4, 3.5 and 4.6 GHz respectively	[18]
EBG-CS at 1.6 GHz vs GPR EBG antenna	11 mm 24.1 mm	0.7 mm 1 mm	3.5 mm 6.3 mm	11.5 cm^3 63 cm^3	One band at 1.6 GHz One band at 1.5 GHz	[19]

(a) (b) (c)

Figure 10. Model of a human hand used to compute the SAR due to exposition to both 4G and WLAN waves.

Table 3. Tissues dielectric properties for human hand SAR calculation.

Tissue	Skin	Muscle	Bone
Permittivity	34.5	58.5	8
Conductivity (S/m)	0.6	1.21	0.105
Density (kg/m^3)	1100	1040	1850

improve this work, a human hand model was developed (Fig. 10), albeit with slight simplifications, by considering only the skin, muscles and bones, for SAR calculation. Fig. 10(c) shows a particular section of the hand which is the most exposed part of the human body due to its proximity to the device's antenna.

In order to accurately simulate the hand exposure to electromagnetic waves using our proposed antenna, the dielectric properties of the selected tissues have to be chosen according to the antenna operating frequencies. In this case, the tissues dielectric properties, which are frequency dependent, must be valid over a range of frequencies encompassing the two antenna operating bands, thus they were chosen to cover a frequency window that ranges from 3 GHz to 6 GHz. Details are presented in Table 3.

The maximum SAR value and cartographies are shown in Table 4 and Fig. 11, respectively.

Table 4. SAR peaks inside the modelled hand tissues when exposed to 4G and WLAN.

	SAR (1g Avg)	SAR (10g Avg)	Gain	Frequency
Without EBG	32.8 W/kg	16.81 W/kg	8.01 dBi	3.5 GHz
With EBG mushroom	2.73 W/kg	1.29 W/kg	3.86 dBi	3.5 GHz
With the proposed EBG-CS	19.1 W/kg	8.21 W/kg	6.71 dBi	3.5 GHz
Without EBG	18.4 W/kg	9 W/kg	6.76 dBi	4.5 GHz
With EBG mushroom	8.65 W/kg	5.35 W/kg	4.87 dBi	4.5 GHz
With the proposed EBG-CS	4.91 W/kg	3.02 W/kg	4.58 dBi	4.5 GHz

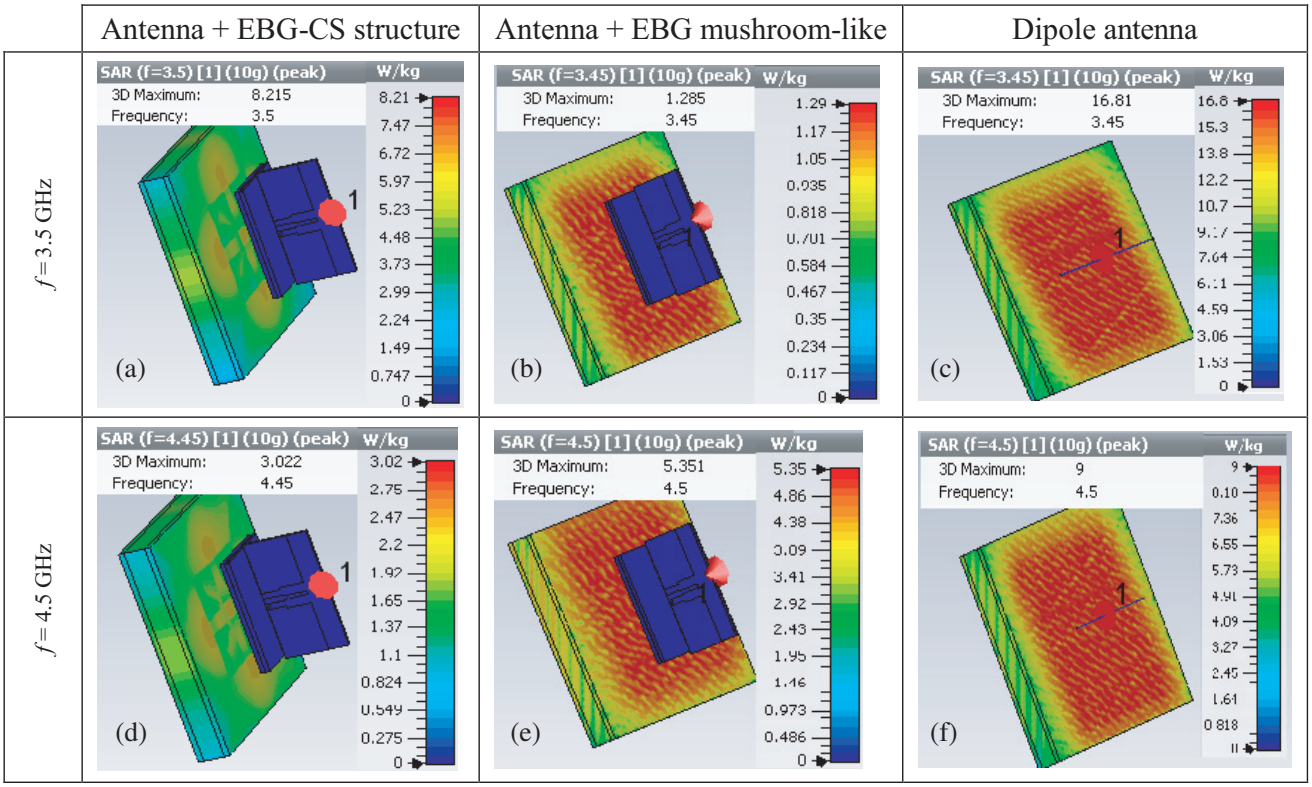

Figure 11. The SAR cartography due to the exposition to both 4G and WLAN waves of the fabricated antenna compared with single dipole antenna. SAR due to: (a) the antenna and EBG-CS structure at 3.5 GHz, (b) the antenna and EBG mushroom like structure at 3.5 GHz, (c) the dipole antenna at 3.5 GHz, (d) the antenna and EBG-CS structure at 4.5 GHz, (e) the antenna and EBG mushroom like structure at 4.5 GHz, (f) the dipole antenna at 4.5 GHz.

Another extremely important issue that needs to be addressed is the SAR value on the device-holding hand in case of using both Wi-Fi (4.5 GHz) and LTE Advanced (3.5 GHz). Considering a situation where the device is held, while communicating with earphones, and at the same time navigating using Wi-Fi, the SAR will then be a combination of both radiation sources, which will be our next perspective. Fig. 11 shows the SAR cartography results at 3.5 GHz (4G) and 4.5 GHz (WLAN). It is necessary to underline that all SAR results presented in this paper will be highly attenuated when the antenna is used inside the phones' or tablets' manufacturing profile and with its appropriate power feeding.

5. CONCLUSION

This work focuses on the redesign of EBG structures, combined with a superstrate, to improve the performance of antennas for mobile applications. A new configuration of EBG antennas was proposed which led to the originality of this paper. This new aspect manifests itself by reaching a dual-band antenna by means of an antenna-EBG-superstrate configuration and successful validation by experimental measurements. The measurement curve shows that the proposed EBG-CS structure reaches a good S_{11} (dB) at the resonance frequency, as well as a significant improvement in bandwidth. Moreover, with the fabricated EBG-CS antenna, a low profile device has been achieved. Finally, the electromagnetic interaction between the proposed EBG-antenna and biological tissues was studied for SAR evaluation.

ACKNOWLEDGMENT

The authors gratefully acknowledge the Erasmus scholarship support provided by the Erasmus Mundus EU-MARE NOSTRUM Program.

REFERENCES

1. Sievenpiper, D., L. Zhang, R. F. J. Broas, N. G. Alexópolous, and E. Yablanovitch, "High-impedance electromagnetic surfaces with a forbidden frequency band," *IEEE Transactions on Microwave Theory and Techniques*, Vol. 47, No. 11, 2059–2074, 1999.
2. Yang, F. and Y. Rahmat-Samii, "A low profile circularly polarized curl antenna over an EBG surface," *Microwave Optical Tech. Lett.*, Vol. 31, No. 4, 264–7, 2001.
3. Yang, F., and Y. Rahmat-Samii, "Microstrip antennas integrated with Electromagnetic Band-Gap (EBG) structures: A low mutual coupling design for array applications," *IEEE Transactions on Antennas and Propagation*, Vol. 51, No. 10, 2003.
4. Yang, F. and Y. Rahmat-Samii, "Reflection phase characterization of an Electromagnetic Band-Gap (EBG) surface," *Proc. IEEE AP-S Dig.*, Vol. 3, 744–747, 2002.
5. Elsheakh, N., H. A. Elsadek, and E. A. Abdallah, "Investigated new embedded shapes of electromagnetic band gap structures and via effect for improved microstrip patch antenna performanced," *Progress In Electromagnetics Research B*, Vol. 20, 91–107, 2010.
6. Gujral, M., J. L.-W. Li, T. Yuan, and C.-W. Qiu, "Bandwidth improvement of microstrip antenna array using dummy EBG pattern feedline," *Progress In Electromagnetics Research*, Vol. 127, 79–92, 2012.
7. Bucci, O. M., T. Isernia, and A. F. Morabito, "Optimal synthesis of circularly symmetric shaped beams," *IEEE Transactions on Antennas and Propagation*, Vol. 62, No. 4, 1954–1964, 2014.
8. Ikeuchi, R. and A. Hirata, "Dipole antenna above EBG substrate for local SAR reduction," *IEEE Antennas and Wireless Propagation Letters*, Vol. 10, 904–906, 2011.
9. Zhang, J., J. Wang, M. Chen, and Z. Zhang, "RCS reduction of patch array antenna by Electromagnetic Band-Gap structure," *IEEE Antennas and Wireless Propagation Letters*, Vol. 11, 1048–1051, 2012.
10. Kurra, L., M. P. Abegaonkar, A. Basu, and S. K. Koul, "Switchable and tunable notch in ultra-wideband filter using electromagnetic bandgap structure," *IEEE Microwave and Wireless Components Letters*, Vol. 24, No. 12, 2014.
11. El Ghabzouri, M., A. Es Salhi, and P. M. Mendes, "New technique to drive the central frequency and to improve bandwidth of EBG structures," *IEEE Mediterranean Microwave Symposium 2015 (MMS 2015)*, Lecce, Italy, 2015.
12. El Ghabzouri, M., A. Es Salhi, and P. M. Mendes, "Shifting the half wave dipole antenna resonance using EBG structure," *IEEE International Conference of Microelectronics 2015 (ICM 2015)*, Casablanca, Morocco, 2015.

13. Yang, F. and Y. Rahmat-Samii, *Electromagnetic Band Gap Structures in Antenna Engineering*, Cambridge University Press, 2008.
14. Fallah, M., F. Hojat-Kashani, and S. H. M. Armaki, "Side effect characterization of EBG structures in microstrip patch antenna," *PIERS Proceedings*, 323–326, Cambridge, USA, July 5–8, 2010.
15. Alam, M. S., M. T. Islam, and N. Misran, "A novel compact split ring slotted electromagnetic band gap structure for microstrip patch antenna performance enhancement," *Progress In Electromagnetics Research*, Vol. 130, 389–409, 2012.
16. Ikeuchi, R., K. H. Chan, and A. Hirata, "SAR and radiation characteristics of a dipole antenna above different finite EBG substrates in the presence of the realistic head model in the 3.5 GHz band," *Progress In Electromagnetics Research B*, Vol. 44, 53–70, 2012.
17. Kulkarni, V. A. and V. S. Navale, "Performance measurement of polarization diversity printed dipole antenna using hight frequency pin diode for WLAN," *International Journal of Advanced Research in Electrical, Electronics and Instrumentation Engineering*, Vol. 2, 1917–1923, 2013.
18. Ma, X., S. Mi, and Y. H. Lee, "Design of a microstrip antenna using square Sierpinski fractal EBG structure," *IEEE 4th Asia-Pacific Conference on Antenna and Propagation (APCAP)*, 2015.
19. McMichael, I. T., E. C. Nallon, V. P. Waymond, R. Scott, Jr., and M. S. Mirotznik, "EBG antenna for GPR colocated with a mital detector for landmine detection," *IEEE Geoscience and Remote Sensing Letters*, 1–5, 2013.
20. Kaharpardeshi, K. T., S. UvaidUllah, and S. Zafar, "Influence of circular patched EBG substrate on SAR and far-field pattern of dipole phase-array antenna," *2014 IEEE Students' Conference on Electrical, Electronics and Computer Science, SCEECS*, 2014.
21. Printed dipole antenna with integrated balun, CST 2014.
22. IEEE Std C95.1^{TM}-2005 (Revision of IEEE Std C95.1-1991), April 19, 2006.
23. Rahim, T. and J. Xu, "Design of high gain and wide band EBG resonator antenna with dual layers of same dielectric superstrate at X-bands," *Journal of Microwaves, Optoelectronics and Electromagnetic Applications*, Vol. 15, No. 2, 2016.
24. Hoang, T. V., T. T. Le, Q. Y. Li, and H. C. Park, "Quad-band circularly polarized antenna for 2.4/5.3/5.8 GHz WLAN and 3.5 GHz WiMAX applications," *IEEE Antennas and Wireless Propagation Letters*, Vol. 15, 1032–1035, 2015.
25. Ayop, O. and M. K. A. Rahim, "Analysis of Mushroom-like electromagnetic band gap structure using suspended transmission line technique," *2011 IEEE International RF and Microwave Conference (RFM 2011)*, Seremban, Malaysia, 2011.